Site preferences and ordering in Nb(Al_{1-x} M_x)₂ (M = Ni or Cu) ternary Laves phases

George Kim, Qing Gu, Philip Nash, and Wei Chen*

Department of Mechanical, Materials, and Aerospace Engineering,

Illinois Institute of Technology, Chicago, IL 60616, USA

Abstract

The properties of binary Laves phases can often be improved by incorporation of additional elements into the crystal structure. In some cases, only a ternary Laves phase exists in an alloy system but with a substantial homogeneity range. Knowledge of the site preference in these compositionally complex intermetallics is necessary to tune the properties for improved performance. The site preferences and substitutional ordering behavior of two ternary C14 Laves phases Nb(Al_{1-x}Ni_x)₂ and Nb(Al_{1-x}Cu_x)₂ are studied with first-principles cluster expansion and Monte Carlo simulations. The ternary Laves phases show extended solubility ranges with constant Nb concentration from experiments, but do not have binary Laves analogues AB_2 in their respective systems. At low alloying concentrations the alloying elements Ni and Cu have preferences for the 6h B-sites in the respective Nb(Al_{1-x}Ni_x)₂ and Nb(Al_{1-x}Cu_x)₂ Laves phases. At higher alloying concentrations (x > 0.25), Cu atoms are distributed with a slight preference for the 6h B-sites, but the Ni atoms show higher preferences for the 2a B-sites. Pair correlation analysis from the Monte Carlo simulations show that both Laves phases prefer heteroatomic 1st and 2nd nearest neighbor pairs. Drop-synthesis calorimetry experiments and first-principles calculations of formation enthalpies as a function of composition are found to be in good

agreement. The Monte Carlo simulation also show that the site preferences of the alloying element depend on the preference of homoatomic bond pair-types on the Kagome layers formed by *6h* atoms.

Keywords: Alloys, ab initio calculation, Enthalpy of formation, Atomic ordering, Laves phases *Corresponding author: wchen66@iit.edu

1. Introduction

Laves phases make up the largest class of intermetallic compounds with more than 1400 binary and ternary members [1,2]. Stoichiometric binary Laves phases, AB_2 , have distinct topologically close-packed atomic configurations as in three main crystal structures: C15 (face centered cubic with the prototype MgCu₂), C14 (hexagonal with the prototype MgZn₂), and C36 (hexagonal with the prototype MgNi₂) [3]. Many Laves phase compounds have important applications such as anodes for batteries [4], hydrogen storage [5,6] and as strengthening phases in structural alloys [7–9]. However, a major issue of Laves phases is their low-temperature brittleness [10], which has motivated numerous studies to understand these phases from the viewpoint of processing conditions [11,12], ternary alloying, and deformation behaviors [13,14]. Different from binary Laves phases that have limited homogeneity ranges, ternary Laves phases can be stable over substantial compositional ranges, which offers the opportunity to tune the properties of the compound to improve performance. For example, there are reports of increased ductility in offstoichiometric Laves phases [15–18]. As of yet there is no general rule to predict the solubility of alloying elements in Laves phases or the compositional dependence of mechanical

properties[13]. In addition, compositional and temperature dependent phase transformations can also take place between different Laves phase polytypes [1,3]. TiCo₂ and ZrFe₂ are examples of Laves phases with compositional dependent polytypic stability. These Laves phases are cubic C15 structure at stoichiometric compositions but undergo a structural transformation into the C36 structure with higher concentrations of Co and Fe respectively [1]. Other Laves phases, such as the C14 Laves phase TaFe₂, can have large homogeneity ranges extending on both the A- and B-rich side of the stoichiometric composition without changing polytypes [1]. The substitutional preferences and (dis)ordering of alloying elements affect the stability and atomic interactions in ternary Laves phase, which is critical in the design of new Laves phase structures for functional or structural applications [19–22].

Alloying a third element in the Laves phase introduces lattice distortions that can lead to site-occupancy preferences or ordering [23]. Binary Laves phases with an ideal radius ratio $\frac{r_A}{r_B} = \sqrt{3/2} \approx 1.225$ and ideal atomic coordinates have the *A*-site Voronoi cell 23% larger than the *B*-site Voronoi cell [3]. A range of radius ratios from 1.05 to 1.68 has been observed in Laves phase compounds [23]. Alloying elements with atomic radii closer to the A(or B) element would be expected to substitute the A(or B)-sites. The limitation of this simple rule is that it cannot make strong predictions when the *A* and *B* radius is similar or the radius of the alloying element lies halfway between those of *A* and *B*. Additionally, in the *C*14 and *C*36 Laves phases there are symmetrically inequivalent *B* sites with equal Voronoi volume. The single-parameter rule based on the atomic radius is unable to make predictions considering the different coordination of the *B*-sites. For example, the size-effect rule cannot predict the switching of site-preference in Cr- or Mn- alloyed NbFe₂ where the alloying elements prefer the 2*a B*-sites at low alloying

concentrations but change to the 6h B-sites at higher concentrations. Such site occupation reversal exists in certain ternary Laves system where the preferred sites of the alloying elements are compositionally dependent [24,25]. General rules based on electronegativity differences or valence electron concentrations have not been found either [3]. Pair interactions may be able to partially explain the compositional dependence of site preferences [3,26,27]. However, the strengths of these pair interactions are often not known and requires quantitative methods to study them.

In this work we study the ternary Nb(Al_{1-x} M_x)₂ (M = Ni or Cu) C14 Laves phases. A description of the C14 Laves structure, the nearest neighbor (NN) bonds, and coordination polyhedral in an ideal C14 Laves structure is shown in Fig. 1. The atoms and bonds are color-coded by the Wyckoff positions and the NN order. The plane of the 6h sites form a Kagome net where the cyan, blue, and purple bonds represent the 1st NN bonds between the 6h sites, the 2nd NN bonds between the 6h sites and the 2a sites above the plane of 6h sites, and the 3^{rd} NN bonds between the 6h sites respectively.

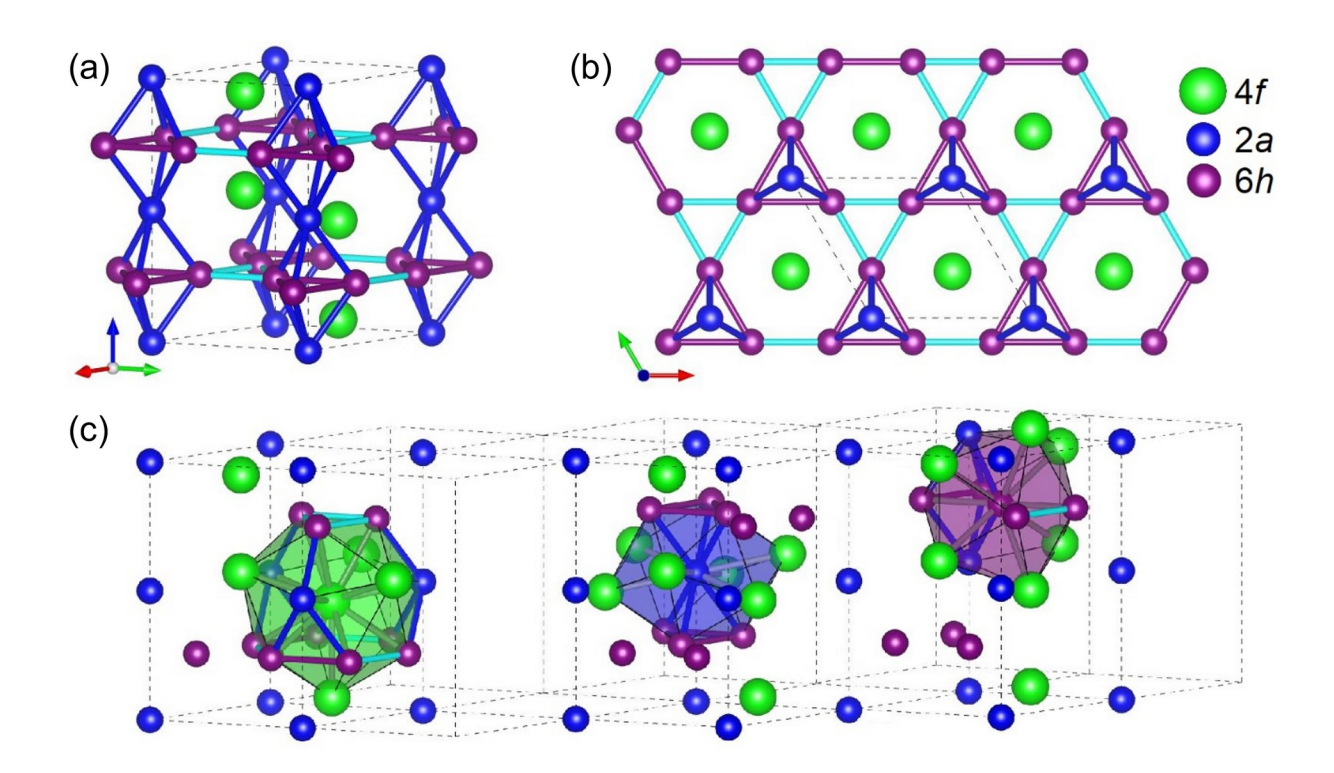


Figure 1. (a) The C14 unit cell is shown with dashed lines with the Wyckoff label 4f, 2a and 6h sites represented by the neon green, blue, and purple atoms respectively. The 1^{st} , 2^{nd} , and 3^{rd} NN bonds are represented by the cyan, blue and purple bonds respectively. (b) The layers of 6h sites form a Kagome net, the 2a and 4f atoms shown are above the Kagome net plane. (c) From left to right the coordination polyhedra shown are centered around the 4f site, 2a site, and 6h sites in the C14 Laves phase.

The Nb(Al_{1-x} M_x)₂ (M = Ni or Cu) Laves phases are considered "true" ternary Laves phases as they have no stable binary Laves counterparts in any of the binary subsystems rather than being binary Laves phases that have extended solubility ranges with the alloying element. These two phases were experimentally found to have extensive homogeneity ranges as shown in the phase diagrams in Fig. 2 [28,29].

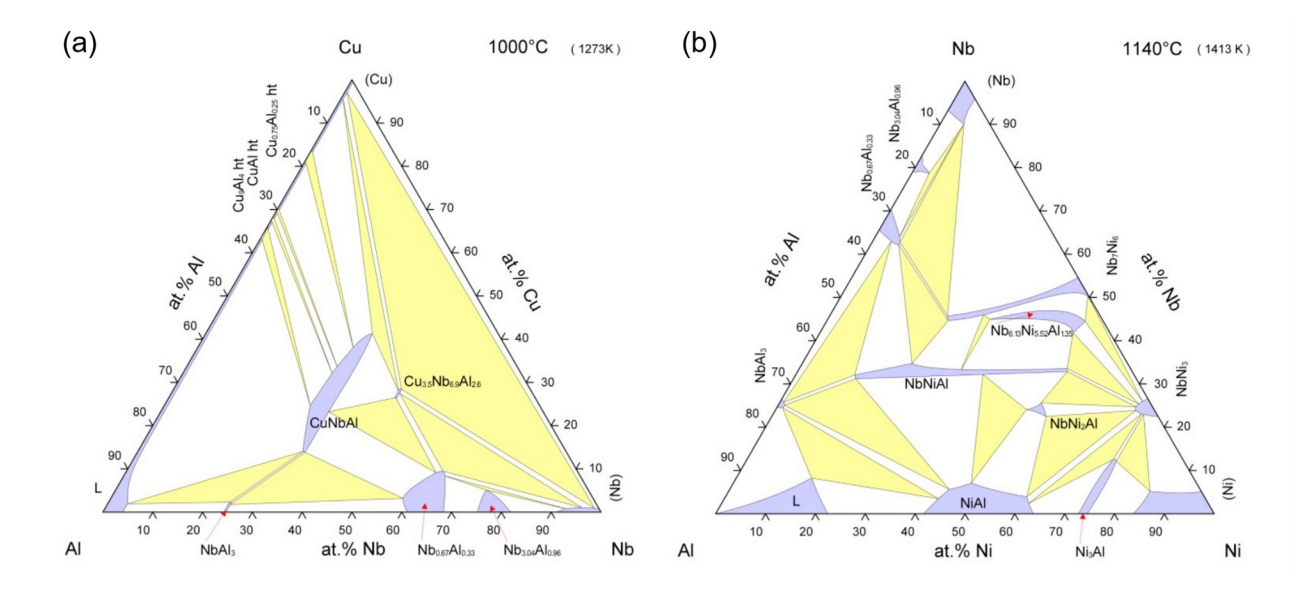


Figure 2. Experimental ternary phase diagram for the (a) Nb-Al-Cu system at 1273 K [28] and (b) Nb-Al-Ni system at 1413 K [29].

The extension of the Laves phase field along an almost constant Nb content indicates that the site substitution preference is for the B atoms. Metallic Cu and Ni have similar atomic radii of 1.28 Å and 1.24 Å, respectively, and the alloying of Cu or Ni brings the atomic radius ratio closer to the ideal value of 1.225. The atomic radius ratios $\frac{r_{Nb}}{r_B}$ where B is Al, Cu, and Ni are 1.007, 1.123, and 1.160 respectively. We utilize first-principles cluster expansions (CE) and Monte Carlo simulations to investigate the site preferences and substitutional ordering of the Al/Ni and Al/Cu species on the B sites. The ordering on the B sites can be understood from the chemical interactions with the substitutional elements. Additionally, the experimental calorimetry and diffraction characterizations are compared to computational results.

2. Methods

2.1. First-principles Cluster Expansions

Finding low-energy structures by direct calculations of all ordered structures in the Nb(Al_{1-x} M_x)₂ (M= Ni, or Cu) phases from first-principles is infeasible because of the large configurational space defined by the atomic arrangements of two species on the B sites of the ternary Laves phases. The CE formalism is a well-established approach to solve the alloy ordering problem and can quickly locate low-energy configurations[30–33]. CE employs a generalized Ising model that parametrizes the enthalpy of formation ΔE of a configuration σ as the summation of weighted cluster correlation functions based on the products of occupation variables σ_i . J_α is a weight coefficient called the effective cluster interaction (ECI) for the cluster α . Using a chosen set of

clusters, the energy of a structure with a configuration σ given by occupation variables σ_i is predicted using Eq. 1.

$$\Delta E(\sigma) = \sum_{\alpha} m_{\alpha} J_{\alpha} \prod_{i \in \alpha'} \sigma_{i} \tag{1}$$

where m_{α} is the multiplicity of the cluster α .

First-principles calculations of training structures are performed to build an accurate CE Hamiltonian with which the ground-state ordering can be efficiently predicted by evaluating the formation energy of a large number of configurations. The ECI values are fitted to predict the energy of a given configuration represented by a vector of correlation functions defined for the chosen clusters of the CE. For a binary ordering problem, the obtained ECI values for a set of clusters sometimes can be used to describe the ordering and clustering behavior of the atomic species. In this study, the CE was constructed using the Alloy Theoretic Automated Toolkit (ATAT) [34–38]. In total, 215 training structures were calculated for the Nb(Al_{1-x}Cu_x)₂ Laves system, and 181 training structures were calculated for the Nb(Al_{1-x}Cu_x)₂ Laves system. The ground state search considered all supercells containing at most 36 atoms. The Cu and Ni atoms in the Laves phase were assumed to be exclusively on the *B*-sites.

The total energy calculations were performed with density functional theory (DFT) using the projector augmented wave (PAW) method as implemented in the Vienna Ab-initio Simulation Package (VASP). A plane-wave cutoff energy of 520 eV and gamma-centered *k*-point meshes with a density of 5000 k-points per reciprocal atom were used. The exchange-correlation energy was approximated with the Perdew-Burke-Ernzerhof (PBE) generalized-gradient approximation

(GGA) functional. All structures were optimized until the energy was converged within 10⁻⁵ eV per supercell.

2.2. Monte Carlo simulations

To examine the site occupancy and ordering tendency at finite temperatures, canonical Monte Carlo simulations were performed for the ternary Laves systems with the cluster expansion Hamiltonian. The Monte Carlo simulations were run using the ATAT emc2 package at a temperature of 300K, using supercells with 4,800 atoms with random initializations and at least ten million Monte Carlo equilibrium and averaging steps. After the cluster correlation fluctuations became small and converged around average values, the compositional occupancy of the 2a and 6h sites, and the 1st, 2nd, and 3rd NN pair correlations are calculated. Monte Carlo snapshots were also analyzed to extract the NN pair-type fractions.

2.3. Experimental formation enthalpy measurement and XRD measurements

The formation enthalpies of selected Nb(Al_{1-x} M_x)₂ (M = Ni or Cu) compositions were measured using drop-calorimetry experiments. Details of the drop-calorimetry methodology can be found in reference [39]. All samples were prepared with high purity metal powder. The sources and purity are listed in Table 1.

Table 1. The purity, source and particle size of all powders

	Purity (wt %)	Co.	Size
Nb		Johnson Matthey Chemicals Limited	
Al	99.97%	Alfa Aesar	~325 mesh

Ni	99.999%	Alfa Aesar	~325 mesh
Cu	99.999%	Alfa Aesar	~100 mesh

The Ni and Cu powders were each reduced at 823 K for an hour in a furnace with flowing hydrogen to remove oxides. The reduced powders were then ground and sieved to ~325 mesh. All powders and samples were stored in a vacuum desiccator. The powders were mixed after weighing, and then compressed into small pellets. Multiple samples were synthesized for each composition to determine experimental uncertainty. Five different Nb(Al_{1-x}Ni_x)₂ compositions were synthesized, with 8 samples made for each composition. Four different Nb(Al_{1-x}Cu_x)₂ compositions were synthesized with 11 samples made for each composition. The enthalpy of formation was measured using a Setaram LIGNE 96 drop calorimeter. After all the samples were reacted, they were cooled within the calorimeter under Argon gas. The reference material used to calibrate the formation energy was sapphire (NIST SRM 720 Synthetic Sapphire, α-Al2O3) [40]. To determine the crystal structure and lattice parameters, GSAS[41] was used to perform Rietveld refinement on the XRD patterns of the synthesized compositions. For the Nb(Al_{1-x}Ni_x)₂ compositions, additional samples were arc melted and homogenized at 1100 °C for 168 h and water quenched to obtain the XRD patterns. For each composition, one synthesized sample was analyzed using scanning electron microscopy (SEM) and energy-dispersive spectroscopy (EDS) to verify the compositions and check for secondary phases.

3. Results

3.1. Cluster expansions

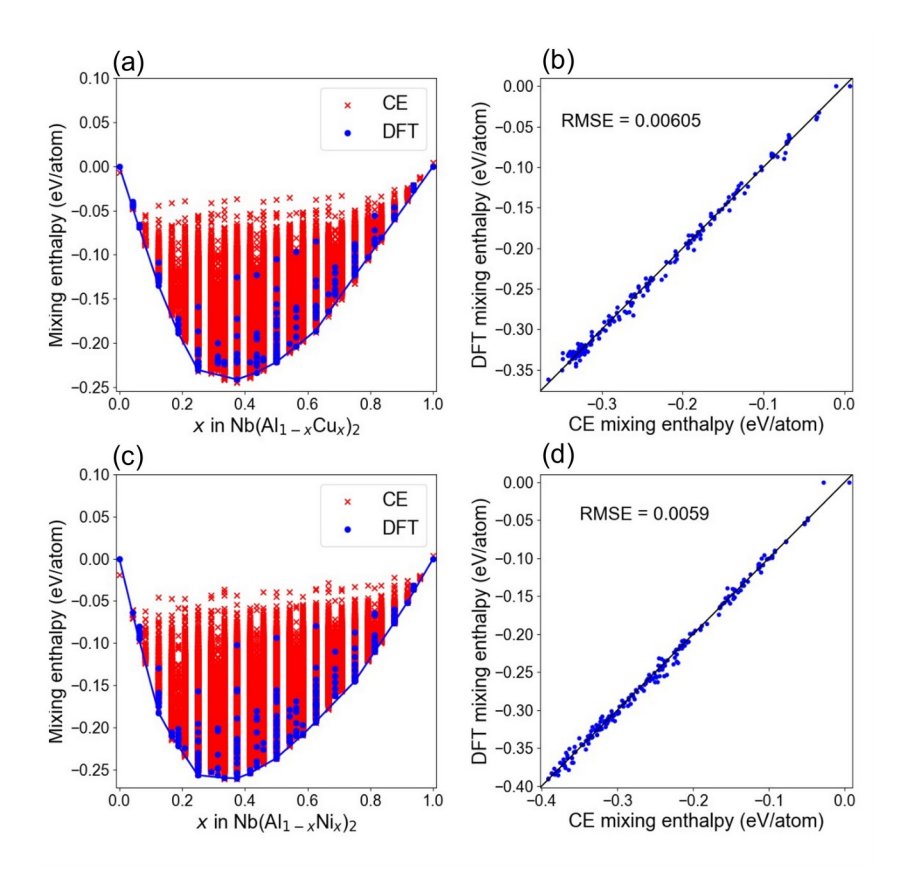


Figure 3. (a) and (c) are the DFT mixing enthalpies, CE predicted mixing enthalpies, and the DFT convex hull for the Nb(Al_{1-x}Ni_x)₂ and Nb(Al_{1-x}Cu_x)₂ Laves phases respectively. (b) and (d) compare the CE fitted mixing enthalpies with DFT values for the Nb(Al_{1-x}Ni_x)₂ and Nb(Al_{1x}Cu_x)₂ phases respectively.

A CE was constructed for each ternary Laves system $Nb(Al_{1-x}Ni_x)_2$, and $Nb(Al_{1-x}Cu_x)_2$. The CE models were converged with a tolerance of 8 meV/atom in evaluating the agreement between DFT and CE convex hull. The CE models have a leave-one-out cross-validation (LOOCV) score of 11.42, and 7.67 meV/atom and their mixing enthalpy predictions had a root-mean-squared

error (RMSE) of 5.90 and 6.04 meV/atom respectively. Fig. 3 (a) and (c) shows the predicted mixing enthalpies of the enumerated configurations as red crosses, the DFT calculated structures as blue dots, and the ground state convex hull formed by the DFT calculated structures represented by the blue line curve. The fitting accuracy of the CE models is shown in Fig. 3 (b) and (d).

3.2. Comparison of DFT and experimental energies

The Nb(Al_{1-x} M_x)₂ (M = Ni or Cu) phases both have extended homogeneity ranges as shown in the experimental phase diagrams of the Nb-Al-Ni and Nb-Al-Cu ternary systems. The homogeneity range of the Nb(Al_{1-x}Ni_x)₂ phase at 1413 K extends from 13 Al at% to 56 Al at%, with a constant Nb concentration of 33 at%. Similarly, the homogeneity range of the Nb(Al₁- $_{x}Cu_{x}$)₂ phase extends from 25 Al at% to 53 Al at% with a constant Nb concentration of 33 at% at 1273K. The trend of calculated and experimental formation enthalpies versus composition agree well as shown in Fig. 4. The experimental and DFT formation enthalpy comparisons are made in Tables 2 and 3. In Table 4, DFT formation enthalpies of four compositions in each Laves phase, including the two end compositions NbAl₂ and NbM₂, and two intermediate compositions $Nb(Al_{0.75}M_{0.25})_2$ and $Nb(Al_{0.25}M_{0.75})_2$ with configurations such that the alloying elements Ni or Cu completely occupy the 2a and 6h sites respectively are also shown. The largest difference determined as the experimental minus calculated values in the Nb(Al_{1-x}Cu_x)₂ phase occurs at the Nb(Al_{0.74}Cu_{0.26})₂ composition with a difference of -0.060 eV/atom and the largest difference in the Nb(Al_{1-x}Ni_x)₂ phase occurs at the Nb(Al_{0.55}Ni_{0.45})₂ composition with a difference of 0.077 eV/atom. The difference between the calculated and experimental formation enthalpies of the Laves compositions synthesized in this work is smaller than the standard deviation of the

differences in DFT and experimental formation enthalpies analyzed in a previous evaluation formation enthalpy in Ref. [42].

Table 2. Reaction enthalpy (ΔH_r), heat content (ΔH_c), standard formation enthalpy (ΔH_{f298}), and DFT formation enthalpy (ΔH_{DFT}) of Nb(Al_{1-x}Ni_x)₂ Laves phase with different compositions

	Composition	ΔHr	ΔНс	ΔH_{f298}	$\Delta H_{ m DFT}$	Expt DFT
		(eV/atom)	(eV/atom)	(eV/atom)	(eV/atom)	(eV/atom)
1	$Nb(Al_{0.77}Ni_{0.23})_2$	-0.219	0.273	-0.491	-0.513	0.022
		± 0.018	± 0.005	± 0.019		
2	$Nb(Al_{0.7}Ni_{0.3})_2$	-0.209	0.245	-0.454	-0.521	0.067
		± 0.020	± 0.002	± 0.020		
3	$Nb(Al_{0.55}Ni_{0.45})_2$	-0.162	0.259	-0.421	-0.497	0.076
		± 0.020	± 0.004	± 0.020		
4	$Nb(Al_{0.39}Ni_{0.61})_2$	-0.120	0.275	-0.395	-0.437	0.042
		± 0.016	± 0.015	± 0.022		
5	$Nb(Al_{0.24}Ni_{0.76})_2$	-0.111	0.278	-0.389	-0.366	-0.023
		± 0.012	± 0.023	± 0.026		

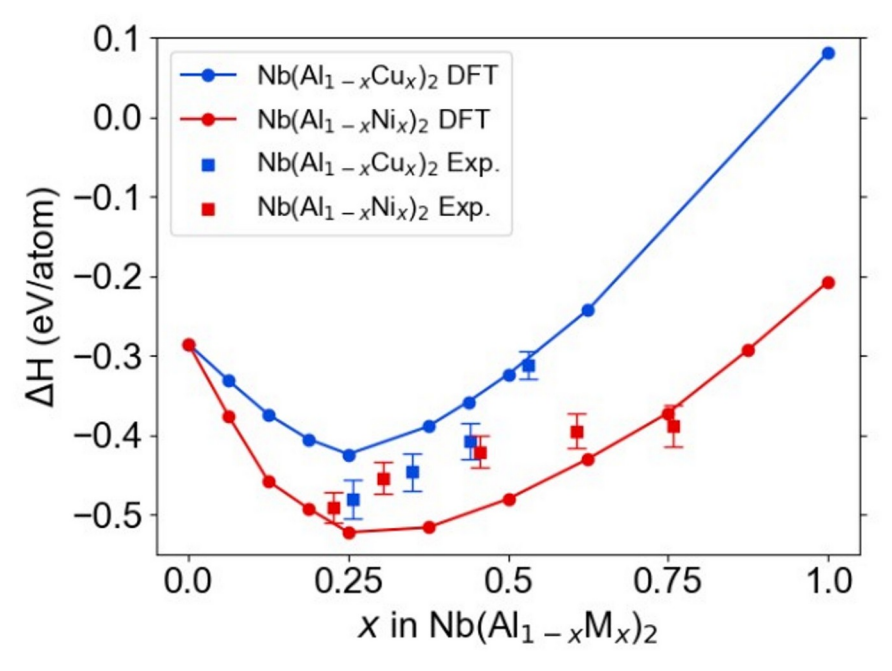
Table 3. Reaction enthalpy (ΔH_r), heat content (ΔH_c), standard formation enthalpy (ΔH_{f298}), and DFT formation enthalpy (ΔH_{DFT}) of Nb(Al_{1-x}Cu_x)₂ Laves phase with different compositions

	Composition	ΔHr	ΔНс	ΔH_{f298}	$\Delta H_{ m DFT}$	Expt DFT
		(eV/atom)	(eV/atom)	(eV/atom)	(eV/atom)	(eV/atom)
1	$Nb(Al_{0.74}Cu_{0.26})_2$	-0.226	0.255	-0.481	-0.421	-0.060
		± 0.013	± 0.020	± 0.024		
2	$Nb(Al_{0.65}Cu_{0.35})_2$	-0.159	0.288	-0.447	-0.389	-0.058
		± 0.012	± 0.019	± 0.023		
3	$Nb(Al_{0.56}Cu_{0.44})_2$	-0.110	0.298	-0.408	-0.357	-0.051
		± 0.016	± 0.017	± 0.023		
4	$Nb(Al_{0.47}Cu_{0.53})_2$	-0.034	0.280	-0.312	-0.304	-0.008
		± 0.003	± 0.018	± 0.018		

Table 4. DFT formation enthalpies (ΔH_{DFT}) of the two end compositions NbAl₂, Nb M_2 (M = Ni or Cu) and the two intermediate compositions Nb(Al_{0.75} $M_{0.25}$)₂ and Nb(Al_{0.25} $M_{0.75}$)₂ for which the alloying elements Ni or Cu completely occupy the 2a and 6h sites respectively.

	Composition	ΔH _{DFT}	Composition	ΔH _{DFT} (eV/atom)
		(eV/atom)		
1	$NbAl_2$	-0.286	$NbAl_2$	-0.286
2	$Nb(Al_{0.75}Ni_{0.25})_2$	-0.518	$Nb(Al_{0.75}Cu_{0.25})_2$	-0.406
3	$Nb(Al_{0.25}Ni_{0.75})_2$	-0.353	Nb(Al _{0.25} Cu _{0.75}) ₂	-0.112
4	$NbNi_2$	-0.207	NbCu ₂	0.082

Figure 4. Comparison of experimental formation enthalpies and the DFT calculated convex hull



in the $Nb(Al_{1-x}Cu_x)_2$ and $Nb(Al_{1-x}Ni_x)_2$ phases respectively. The uncertainty of the experimental values are determined by making 8 or more separate measurements for each composition.

SEM and EDS results found that all synthesized samples of Nb(Al_{1-x}Cu_x)₂ consist solely of the desired Laves phase. The nominal Nb(Al_{1-x}Ni_x)₂ samples, however, contained secondary phases which makes the reported formation enthalpies more indicative; An SEM image of the Nb(Al_{0.7}Ni_{0.3})₂ sample is shown in Fig. 5 and phase fractions of all compositions are shown in Table 5. Considering the relative quality of the experimentally produced samples one must consider the kinetics and thermodynamics of competing phases as well as diffusion of the elemental constituents. For the Nb(Al_{1-x}Cu_x)₂ compounds, the calorimeter temperature of 1000 °C results in the melt of Al prior to reaction. During reaction there is adiabatic heating that may also result in the melt of Cu. This situation will facilitate the formation of the ternary compound through effective mixing. On the other hand, in the Nb(Al_{1-x}Ni_x)₂ system liquid formation will occur only for the Al component since the melting point of Ni is much higher than the calorimeter temperature. As a result, the Nb(Al_{1-x}Ni_x)₂ calorimeter samples contained secondary phases, mostly NiAl and some Nb₂Al, which shows that there is a strong interaction between Ni and Al. The presence of secondary phases reduces the precision for the experimental enthalpy of formation measurements.

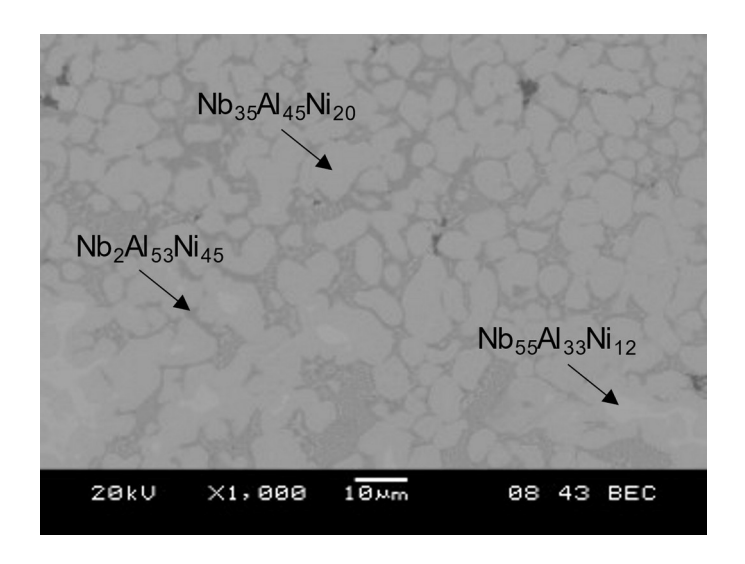


Figure 5. Backscattered electron contrast images (magnification 1000 times) of the nominal Nb(Al_{0.7}Ni_{0.3})₂ composition. Secondary phases including NiAl are found. Details of phase fractions are listed in Table 5.

Table 5. Phase fractions of synthesized Nb($Al_{1-x}Ni_x$)₂ samples.

Composition	Nb(Al _{1-x} Ni _x) ₂	NiAl	Nb ₂ Al
$Nb(Al_{0.77}Ni_{0.23})_2$	0.79	0.20	0.01
$Nb(Al_{0.7}Ni_{0.3})_2$	0.85	0.12	0.03
$Nb(Al_{0.55}Ni_{0.45})_2$	0.90	0.09	0.01
$Nb(Al_{0.39}Ni_{0.61})_2$	0.80	0.18	0.02
$Nb(Al_{0.24}Ni_{0.76})_2$	0.83	0.14	0.03

3.3. Experimental and calculated XRD patterns

XRD patterns were measured at room temperature for each synthesized composition and compared with the simulated XRD patterns of supercell structures with matching compositions, shown in Fig. 6 (a) and (b). For both Nb(Al_{1-x} M_x)₂ (M = Ni or Cu) Laves phase samples, simulated XRD patterns of the lowest energy supercell structures were found to have good agreement with the experimental XRD patterns, with the exception of a small shift in peak positions which is the result of the differences in lattice parameters. The good agreement between the simulated and experimental patterns suggests that substitutional site preference and ordering behavior in the synthesized samples follows the tendency predicted by the Monte Carlo simulations. Due to the secondary phases present in the calorimetry Nb(Al_{1-x}Ni_x)₂ samples, additional samples at the same nominal compositions were arc melted and homogenized at 1100 °C for 168 h and water quenched. These additional Nb(Al_{1-x}Ni_x)₂ samples contained no secondary phases and were used to obtain the XRD patterns.

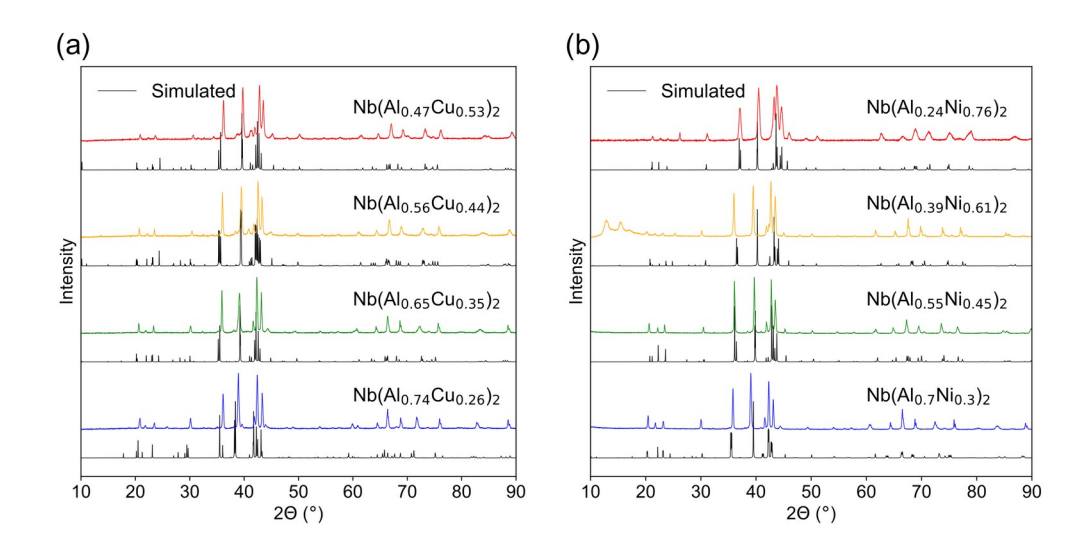


Figure 6. Comparison of experimental and simulated (black) XRD patterns for different (a) Nb(Al_{1-x}Cu_x)₂ and (b) Nb(Al_{1-x}Ni_x)₂ compositions.

3.4. Monte Carlo simulations

The site concentrations for Nb(Al_{1-x} M_x)₂ (M = Ni or Cu) are converted from the point cluster correlations from the Monte Carlo simulations. As shown in Fig. 7, at low alloying concentrations (x < 0.25), Ni and Cu occupy the 2a B-sites at a much lower fraction than if they were distributed proportionally between the 2a and 6b B-sites. The dashed line represents proportional site occupancy corresponding to the overall composition. The alloying elements have a slightly higher preference for the 6b B-sites at low alloying concentrations in the Nb(Al_{1-x}Ni_x)₂ and Nb(Al_{1-x}Cu_x)₂ phases. At higher concentrations, Cu continues to have a slight preference for the 6b sites in the Nb(Al_{1-x}Cu_x)₂ phase, but Ni is found to have a greater preference for the 2a sites for Ni compositions (x > 0.30). Because the ratio of the 6b to 2a sites is 3:1 in a

C14 unit cell, the same concentration change in these sites indicates three times as many 6h atoms than the 2a atoms deviate from the proportional site occupancy.

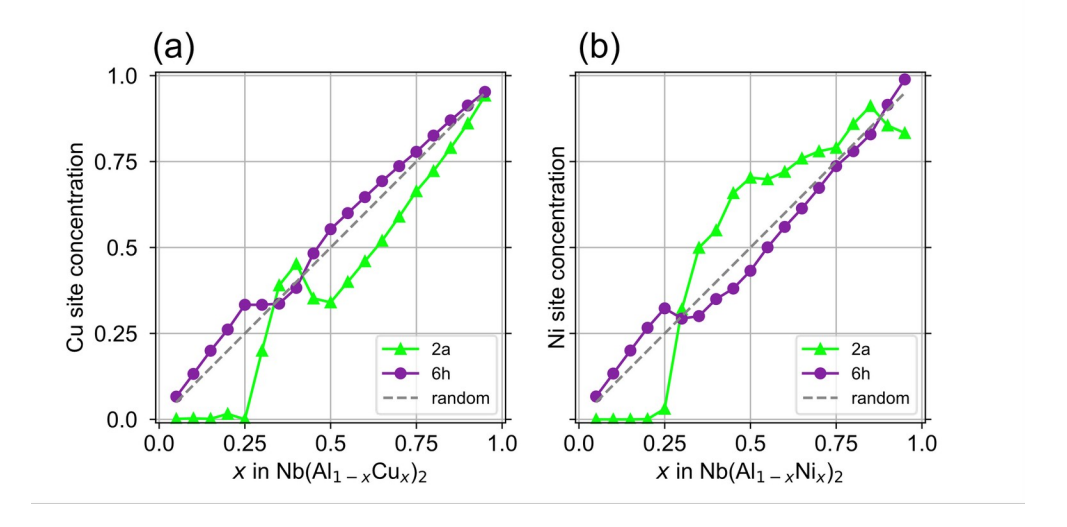


Figure 7. (a) and (b) are the site concentrations of the Cu and Ni atomic species on the 2a and 6h sites in the Nb(Al_{1-x}Cu_x)₂ and Nb(Al_{1-x}Ni_x)₂ phases respectively. The site concentrations the alloying element on the 2a (6h) sites are represented by the neon green (purple) curves. The dashed grey line represents the case in which the alloying elements occupy equal proportions of the 2a and 6h sites.

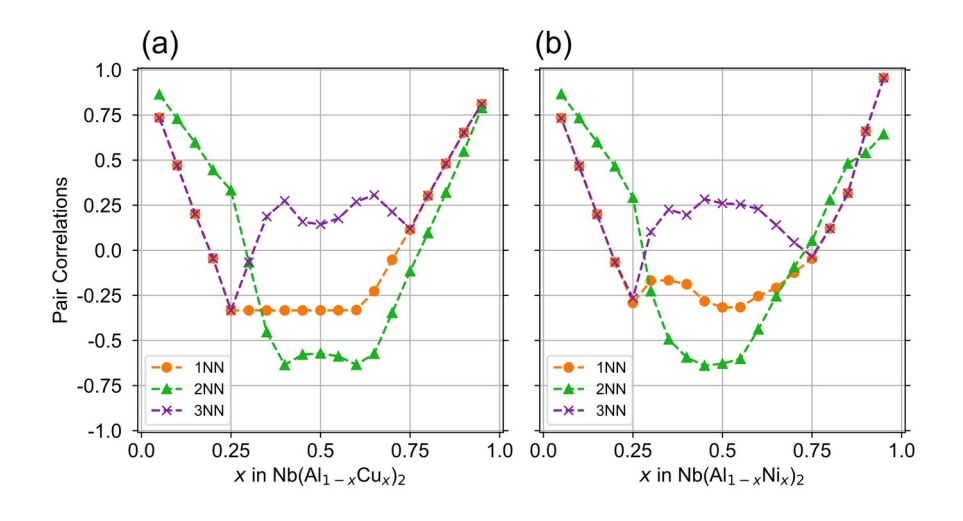


Figure 8. 1st, 2nd, and 3rd NN pair cluster correlations for the (a) Nb(Al_{1-x}Cu_x)₂ and (b) Nb(Al_{1-x}Ni_x)₂ phases calculated from Monte Carlo simulations.

A negative pair cluster correlation corresponds to the pair consisting of more unlike species while a positive pair cluster correlation corresponds to the pair consisting of more like species. Pair cluster correlations from the Monte Carlo simulations are plotted in Fig. 8, which shows that in both the Ni and Cu systems the 1st, and 2nd NN pair cluster correlations are negative in the composition range 30-70%, while the 3rd NN pair cluster correlations are positive for most of the compositions in both systems.

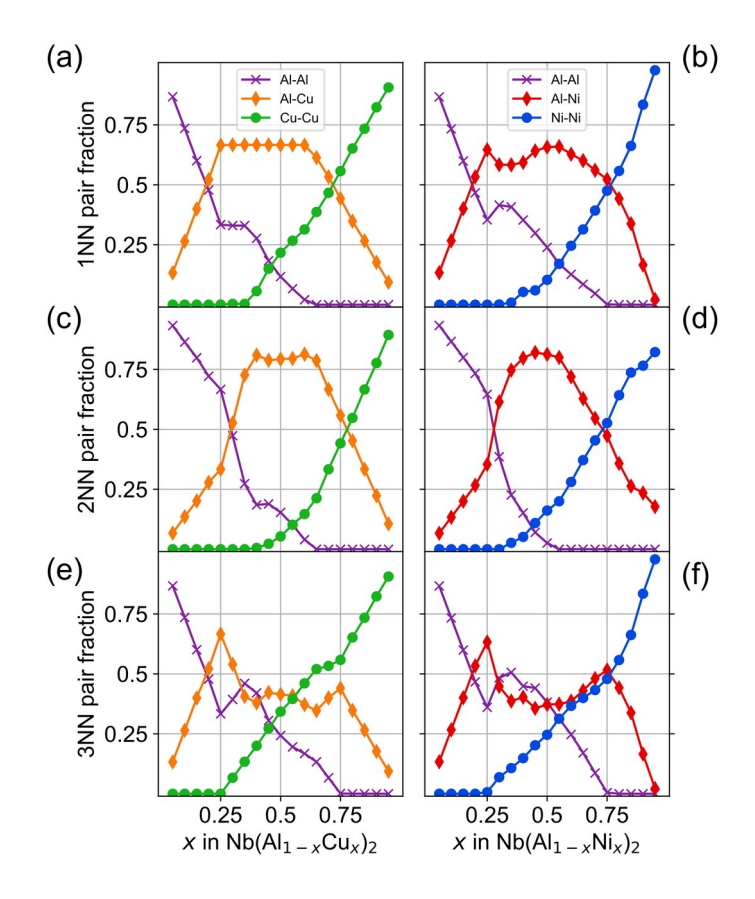


Figure 9. (a), (b) Curves showing the compositional dependence of the relative frequency of 1st NN atomic pair types. (c), (d) The compositional dependence of 2nd NN atomic pair types. (e), (f) The compositional dependence of 3rd NN atomic pair types. (a), (c), (e) plot relative frequencies of pair counts in the Nb(Al_{1-x}Cu_x)₂ phase and (b), (d), (f) plot relative frequencies of pair counts in the Nb(Al_{1-x}Ni_x)₂ phase.

The fractional frequency of different NN pairs from the Monte Carlo snapshots is plotted in Fig. 9. In both systems, a greater relative fraction of 1st and 2nd NN heteroatomic pairs is observed in the intermediate compositions indicating a preference for ordering on the 1st NN 6*h* sites and the 2nd NN 6*h* and 2*a* sites. Also, the 3rd NN homoatomic bond fractions are higher than the 1st NN homoatomic bond fractions in both systems, suggesting that ordering is preferred on the 1st NN 6*h* site triangles of the Kagome net.

4. Discussion

The compositional dependence of the site preferences and substitutional ordering in the ternary Laves phases Nb(Al_{1-x} M_x)₂ (M = Ni or Cu) can be understood from the first-principles calculations and Monte Carlo simulations. The compositional dependence of site preferences is evaluated from site occupancies of Monte Carlo simulation structural snapshots. Ordering tendencies are analyzed using 1st NN, 2nd NN, and 3rd NN pair cluster correlations, the relative frequencies of nearest neighbor atomic pair types, and a LASSO (Least absolute shrinkage and selection operator) regression model.

4.1. Site preferences

As seen in Fig. 7, the alloying elements, Ni and Cu, both have slight preferences for the 6h sites at low alloying concentrations where x < 0.25 in Nb(Al_{1-x} M_x)₂ (M = Ni or Cu). This is because the alloying concentration is low enough to place Ni and Cu on the 6h sites, making heteroatomic 1st and 3rd NN bonds without also creating homoatomic Ni-Ni or Cu-Cu bonds. However, at higher alloying concentrations, differences arise between the two Laves systems. Cu atoms in the Nb(Al_{1-x}Cu_x)₂ Laves phase have a slight preference for the 6h B-sites. However, in the Nb(Al_{1-x}Ni_x)₂ Laves phase, Ni has a preference for the 2a sites. The difference in the site occupancy behavior between these two ternary Laves phases can be understood from the Kagome net of the plane containing the 6h sites and differences in the preferred homoatomic pair types. Fig. 2 (b) shows the Kagome net that cannot have fully ordered 1st and 3rd NN bonds due to geometric frustration. Therefore, even if heteroatomic nearest neighbor bonds are preferred, homoatomic bonds are unavoidable. This situation gives rise to the site preferences we found in the Monte Carlo simulations. From the relative frequency comparison of bond pair types in Fig. 9 we see that in the Ni system at the 50% concentration Al-Al 1st and 3rd NN bonds are preferred over the Ni-Ni 1st and 3rd NN bonds respectively, which can be minimized by placing more Ni atoms on the 2a sites. In the Cu system, on the other hand, at the 50% concentration the Cu-Cu 1st and 3rd NN bonds are preferred over the Al-Al 1st and 3rd NN bonds respectively, which can be minimized by placing more Al atoms on the 2a sites instead.

4.2. Ordering

From the bond pair-type relative frequencies in Fig. 9 and the pair correlations in Fig. 8, we see that there is a stronger preference to have 3rd NN homoatomic pairs and 1st and 2nd NN heteroatomic pairs in both systems. From these observations we reason that Al and the alloying

elements Cu and Ni prefer to order and the difference between the two systems is due to which homoatomic pairs are preferred on the Kagome net planes. In the Cu system, the Cu-Cu homoatomic NN pairs are preferred on the Kagome net, resulting in Cu atoms having a preference for 6h sites giving rise to Cu-Al ordering where the Cu and Al atoms occupy the 6h and 2a sites respectively. Whereas for the Ni system, the Al-Al homoatomic NN pairs are preferred on the Kagome net, resulting in Ni atoms having a preference for 2a sites and a Ni-Al ordering where the Ni and Al atoms occupy the 2a and 6h sites respectively. This ordering behavior is supported by the negative 2NN pair cluster correlations seen in Fig. 8.

Fig. 10 (a) and (b) show the ECI values for the pair, triplet, and quadruplet clusters for the CE corresponding to the Nb(Al_{1-x}Cu_x)₂ and Nb(Al_{1-x}Ni_x)₂ systems respectively. The ECI plots of both CE models show that the 1st through 3rd NN pair clusters are important in determining the energy of the structures in both systems. However, a direct interpretation of ordering behavior from ECI values is complicated due to the fact that other clusters such as the triplets and quadruplets can also involve nearest neighbors and have both positive and negative ECIs.

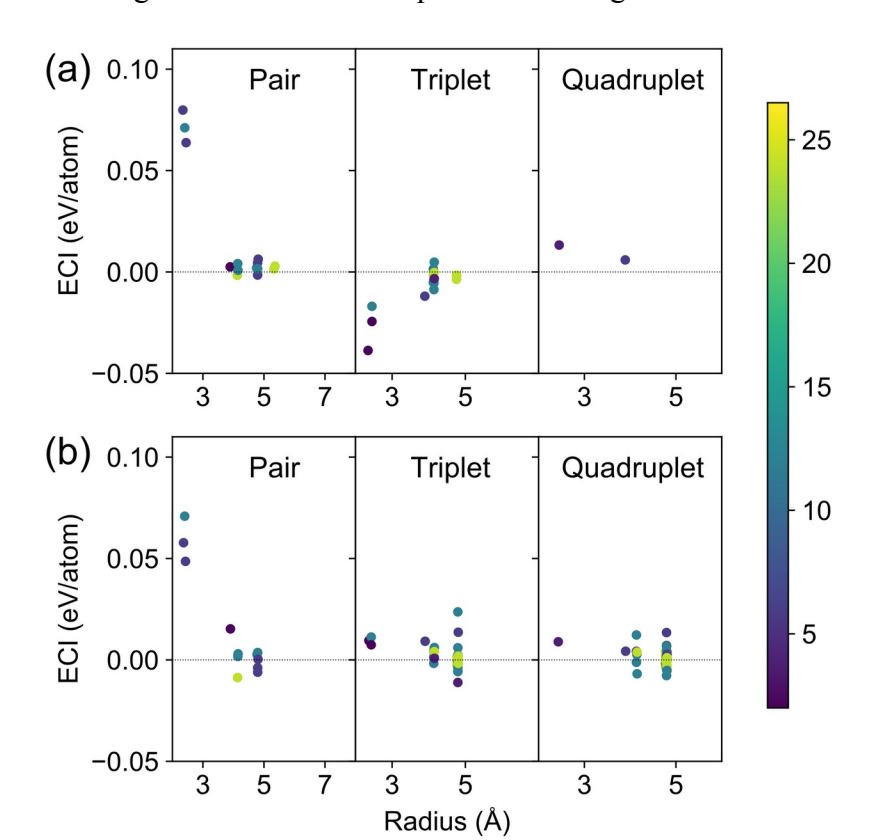


Figure 10. (a) and (b) ECI values of CEs fitted on the Nb(Al_{1-x}Cu_x)₂ and Nb(Al_{1-x}Ni_x)₂ phases respectively. The color bar corresponds to the multiplicity of the clusters.

The relationship between the mixing enthalpies and relative frequencies of bond pair-types of the calculated DFT structures was also investigated using a LASSO linear model implemented with Scikit-learn [43]. Three LASSO models were fitted for each Laves system with L1 regularization parameters, listed in increasing regularization strength, 0.0005, 0.005, and 0.01. The feature coefficients of the LASSO models were then compared and the trends of which features were selected even with stronger regularization parameters was used to gauge their importance. Average cross-validation scores were found using 10-fold cross validation and are listed in Table 6. The prediction target was the mixing enthalpies, and the features used for model predictions were the relative frequencies of the 1st through 9th nearest neighbor bond pair-types. Eq. 5 shows the cost function that is minimized by the LASSO regression for a model fitted on M samples with p features. For each sample i, x is the feature value, w is the coefficient, and λ is the regularization parameter. This regularization, known as L1 regularization, has the effect of producing a sparse model with only the most important features, and giving less significant feature coefficients as zero.

$$\sum_{i=1}^{M} (y_i - \widehat{y}_i)^2 = \sum_{i=1}^{M} \left(y_i - \sum_{j=0}^{p} w_j \times x_{ij} \right)^2 + \lambda \sum_{j=0}^{p} |w_j|$$
(5)

The LASSO model results in Fig. 11 shows the trend of coefficients of features selected by the L1 regularization with increasing regularization strength. The selected features indicate that the homoatomic bonds are not thermodynamically preferred. In the Nb(Al_{1-x}Cu_x)₂ system, the Al-Cu heteroatomic bonds stabilizes the structure. In the Nb(Al_{1-x}Ni_x)₂ system, the mixing enthalpy is

also strongly correlated with the Ni-Ni bond fractions and is to a smaller extent stabilized by the 2^{nd} NN Al-Ni bonds. Reducing 1^{st} , 2^{nd} , and 3^{rd} NN Ni-Ni bonds and increasing the number of 2^{nd} NN Al-Ni bonds can be achieved by placing Ni on the 2a sites. For the Nb(Al_{1-x}Cu_x)₂ phase, the coefficients for the 1^{st} , 2^{nd} , and 3^{rd} NN Al-Cu are all negative which is expected if the Cu atoms have a slight preference for the 6h sites. The site preferences and ordering behavior elucidated from the Monte Carlo simulation results are in good agreement with the simple LASSO model of the DFT calculated structures.

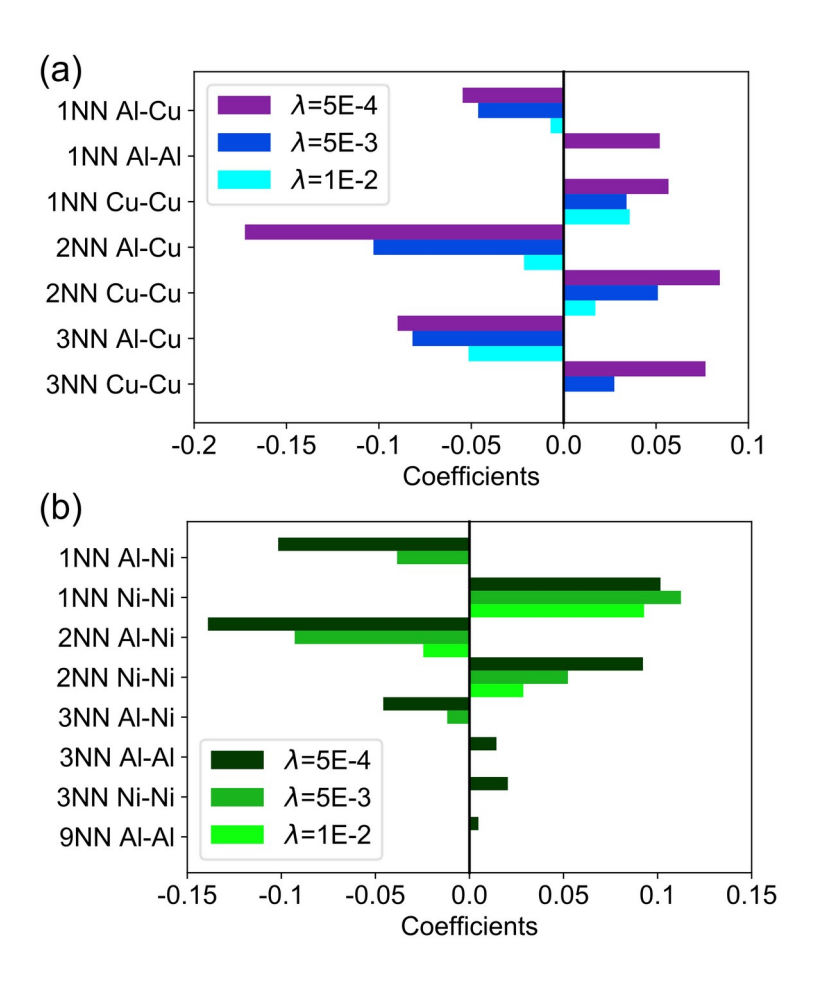


Figure 11. The coefficients of features in the LASSO models fitted on the (a) $Nb(Al_{1-x}Cu_x)_2$ and (b) $Nb(Al_{1-x}Ni_x)_2$ structures The features are the relative frequencies of the nearest neighbor pair types, and the target variable is the mixing enthalpy.

Table 6. RMSE values for LASSO models using different regularization, λ , parameters.

LASSO λ parameter	Nb(Al _{1-x} Ni _x) ₂ CV score (eV/atom)	Nb(Al _{1-x} Cu _x) ₂ CV score (eV/atom)
0.0005	0.03249	0.03362
0.005	0.04641	0.05034
0.01	0.06861	0.07799

Substitutional ordering is present in both Laves phases as shown in the analyses of nearest neighbor pair fractions, the pair cluster correlations of the Monte Carlo simulations, and the LASSO model analysis of the DFT calculated structures. The difference in site preferences and the type of NN bonds involved in the ordering depends on which homoatomic NN bonds are preferred on the Kagome net planes. In the Nb(Al_{1-x}Ni_x)₂ phase, the Al-Al homoatomic bonds are greatly preferred over the Ni-Ni homoatomic bonds, while in the Nb(Al_{1-x}Cu_x)₂ phase it is the Cu-Cu homoatomic bonds that are preferred on the Kagome net planes.

5. Conclusion

The site preferences and ordering behavior in the Nb($Al_{1-x}M_x$)₂ (M = Ni or Cu) ternary Laves phases were studied using first-principles CE models and Monte Carlo simulations. Formation enthalpies, obtained from calorimetry experiments, agree well with the calculated values. Experimentally measured XRD patterns compared with simulated ones from CE predicted ground state structures were found to be similar with minor differences. Analysis of the Monte Carlo simulation results show that at low alloying concentrations (x<0.25), Ni and Cu both have a preference to occupy 6h Wyckoff sites. At higher alloying concentrations in the Nb(Al_{1-x}Cu_x)₂ phase, the Cu species have a slight preference for 6h sites. Whereas, in the Nb(Al_{1-x}Ni_x)₂ phase at higher alloying concentrations, the Ni species has a preference for the 2a sites. This difference in site preferences is due to the preference of Al-Al homoatomic bonds over the Ni-Ni bonds in the Nb(Al_{1-x}Ni_x)₂ phase, while in the Nb(Al_{1-x}Cu_x)₂ phase it is the Cu-Cu bonds that are preferred $_{x}Ni_{x})_{2}$ phases the Cu/Al atoms prefer the 6h sites, allowing for more 1st and 3rd NN homoatomic Cu-Cu/Al-Al bonds. The Al/Ni atoms that prefer the 2a sites then make 2nd NN heteroatomic bonds with the atoms on the 3rd NN 6h site triangles which stabilizes the ternary Laves phases.

Acknowledgements

This material is based upon work supported by the National Science Foundation under Grant No. DMR-1607943 and DMR-1945380.

References

- [1] F. Stein, M. Palm, G. Sauthoff, Structure and stability of Laves phases part II—structure type variations in binary and ternary systems, Intermetallics. 13 (2005) 1056–1074.
- [2] F. Stein, A. Leineweber, Laves phases: a review of their functional and structural applications and an improved fundamental understanding of stability and properties, J. Mater. Sci. (2020).
- [3] F. Stein, M. Palm, G. Sauthoff, Structure and stability of Laves phases. Part I. Critical assessment of factors controlling Laves phase stability, Intermetallics. 12 (2004) 713–720.
- [4] K.-H. Young, S. Chang, X. Lin, C14 Laves Phase Metal Hydride Alloys for Ni/MH Batteries Applications, Batteries. 3 (2017) 27.
- [5] M. Ma, K. Chen, J. Jiang, X. Yang, H. Wang, H. Shao, J. Liu, L. Ouyang, Enhanced hydrogen generation performance of CaMg 2 -based materials by ball milling, Inorg. Chem. Front. 7 (2020) 918–929.
- [6] A. Schneemann, J.L. White, S. Kang, S. Jeong, L.F. Wan, E.S. Cho, T.W. Heo, D. Prendergast, J.J. Urban, B.C. Wood, M.D. Allendorf, V. Stavila, Nanostructured Metal Hydrides for Hydrogen Storage, Chem. Rev. 118 (2018) 10775–10839.
- [7] M. Zubair, S. Sandlöbes, M.A. Wollenweber, C.F. Kusche, W. Hildebrandt, C. Broeckmann, S. Korte-Kerzel, On the role of Laves phases on the mechanical properties

- of Mg-Al-Ca alloys, Mater. Sci. Eng. A. 756 (2019) 272–283.
- [8] G. Qin, Z. Li, R. Chen, H. Zheng, C. Fan, L. Wang, Y. Su, H. Ding, J. Guo, H. Fu, CoCrFeMnNi high-entropy alloys reinforced with Laves phase by adding Nb and Ti elements, J. Mater. Res. 34 (2019) 1011–1020.
- [9] A. Von Keitz, G. Sauthoff, Laves phases for high temperatures—Part II: Stability and mechanical properties, Intermetallics. 10 (2002) 497–510.
- [10] W. Chen, J. Sun, The electronic structure and mechanical properties of MgCu2 Laves phase compound, Phys. B Condens. Matter. 382 (2006) 279–284.
- [11] C.. Liu, J.. Zhu, M.. Brady, C.. McKamey, L.. Pike, Physical metallurgy and mechanical properties of transition-metal Laves phase alloys, Intermetallics. 8 (2000) 1119–1129.
- [12] T. Ohta, Y. Nakagawa, Y. Kaneno, H. Inoue, T. Takasugi, W.Y. Kim, Microstructures and mechanical properties of NbCr2 and ZrCr2 laves alloys prepared by powder metallurgy, J. Mater. Sci. 38 (2003) 657–665.
- [13] W. Luo, C. Kirchlechner, J. Li, G. Dehm, F. Stein, Composition dependence of hardness and elastic modulus of the cubic and hexagonal NbCo 2 Laves phase polytypes studied by nanoindentation, J. Mater. Res. 35 (2020) 185–195.
- [14] W. Luo, C. Kirchlechner, J. Zavašnik, W. Lu, G. Dehm, F. Stein, Crystal structure and composition dependence of mechanical properties of single-crystalline NbCo2 Laves phase, Acta Mater. 184 (2020) 151–163.
- [15] M. Fujita, Y. Kaneno, T. Takasugi, Phase field and room-temperature mechanical properties of C15 Laves phase in Nb–Hf–Cr and Nb–Ta–Cr alloy systems, J. Alloys Compd. 424 (2006) 283–288.
- [16] D.J. Thoma, K.A. Nibur, K.C. Chen, J.C. Cooley, L.B. Dauelsberg, W.L. Hults, P.G.

- Kotula, The effect of alloying on the properties of (Nb,Ti)Cr2 Cl5 Laves phases, Mater. Sci. Eng. A. 329–331 (2002) 408–415.
- [17] Y. Nakagawa, T. Ohta, Y. Kaneno, H. Inoue, T. Takasugi, Defect structures and room-temperature mechanical properties of C15 laves phases in Zr-Nb-Cr and Zr-Hf-Cr alloy systems, Metall. Mater. Trans. A. 35 (2004) 3469–3476.
- [18] T. Ohta, Y. Kaneno, H. Inoue, T. Takasugi, S. Hanada, Phase field and room-temperature mechanical properties of the C15 laves phase in the Zr-Ta-Cr alloy system, Metall. Mater. Trans. A. 36 (2005) 583–590.
- [19] S. Sui, H. Tan, J. Chen, C. Zhong, Z. Li, W. Fan, A. Gasser, W. Huang, The influence of Laves phases on the room temperature tensile properties of Inconel 718 fabricated by powder feeding laser additive manufacturing, Acta Mater. 164 (2019) 413–427.
- [20] Y.W. Chai, K. Kato, C. Yabu, S. Ishikawa, Y. Kimura, Disconnections and Laves (C14) precipitation in high-Cr ferritic stainless steels, Acta Mater. 198 (2020) 230–241.
- [21] Q.X. Long, J. Wang, Y. Du, X.W. Nie, Z.P. Jin, Site occupancy of transition elements in C15 NbCr2 laves phase: A first-principles study, J. Min. Metall. Sect. B Metall. 53 (2016) 20.
- [22] Z. Wei, Y. Yang, J. Huang, B. Wu, B. Sa, Y. Huang, S. Wang, M. Lin, C.-T. Tsai, K. Bai, Prediction of site occupancy of C15 Laves phase at finite temperature based on quasi-harmonic approximation model, Intermetallics. 96 (2018) 33–40.
- [23] T. Yamanouchi, S. Miura, Influence of atomic size factors on the phase stability of laves phase in Nb-Cr-Ni-Al and Nb-V-Ni-Al phase diagrams, Mater. Trans. 59 (2018) 546–555.
- [24] D. Grüner, E. Bischoff, A. Kerkau, A. Ormeci, Y. Prots, H. Borrmann, G. Kreiner, Site occupation reversal in the C14 Laves phase Nb(Cr 1- x Co x) 2, Zeitschrift Für Anorg.

- Und Allg. Chemie. (2008).
- [25] A. Kerkau, D. Grüner, A. Ormeci, Y. Prots, H. Borrmann, W. Schnelle, E. Bischoff, Y. Grin, G. Kreiner, Site occupation reversal in the C14 laves phase Nb(Cr1-xCo x)2, Zeitschrift Fur Anorg. Und Allg. Chemie. 635 (2009) 637–648.
- [26] J.-C. Crivello, J.-M. Joubert, T. Mohri, Atomic interactions in C15 Laves phases, J. Mater. Sci. 54 (2019) 4742–4753.
- [27] M. Šlapáková, A. Zendegani, C.H. Liebscher, T. Hickel, J. Neugebauer, T. Hammerschmidt, A. Ormeci, J. Grin, G. Dehm, K.S. Kumar, F. Stein, Atomic scale configuration of planar defects in the Nb-rich C14 Laves phase NbFe2, Acta Mater. 183 (2020) 362–376.
- [28] P. Villars, H. Okamoto, eds., Al-Cu-Nb Isothermal Section of Ternary Phase Diagram:

 Datasheet from "PAULING FILE Multinaries Edition 2012" in SpringerMaterials

 (https://materials.springer.com/isp/phase-diagram/docs/c 0980741), (n.d.).
- [29] P. Villars, H. Okamoto, eds., Al-Nb-Ni Isothermal Section of Ternary Phase Diagram:

 Datasheet from "PAULING FILE Multinaries Edition 2012" in SpringerMaterials

 (https://materials.springer.com/isp/phase-diagram/docs/c_0976320), (n.d.).
- [30] W. Chen, D. Schmidt, W.F. Schneider, C. Wolverton, First-principles cluster expansion study of missing-row reconstructions of fcc (110) surfaces, Phys. Rev. B. 83 (2011) 075415.
- [31] J.M. Sanchez, F. Ducastelle, D. Gratias, Generalized cluster description of multicomponent systems, Phys. A Stat. Mech. Its Appl. 128 (1984) 334–350.
- [32] W. Chen, D. Schmidt, W.F. Schneider, C. Wolverton, Ordering and Oxygen Adsorption in Au–Pt/Pt(111) Surface Alloys, J. Phys. Chem. C. 115 (2011) 17915–17924.

- [33] W. Chen, P. Dalach, W.F. Schneider, C. Wolverton, Interplay between Subsurface Ordering, Surface Segregation, and Adsorption on Pt–Ti(111) Near-Surface Alloys, Langmuir. 28 (2012) 4683–4693.
- [34] A. van de Walle, G. Ceder, Automating first-principles phase diagram calculations, J. Phase Equilibria. 23 (2002) 348–359.
- [35] A. Van De Walle, M. Asta, Self-driven lattice-model Monte Carlo simulations of alloy thermodynamic properties and phase diagrams, Model. Simul. Mater. Sci. Eng. 10 (2002) 521–538.
- [36] A. Van de Walle, M. Asta, G. Ceder, The alloy theoretic automated toolkit: A user guide, Calphad Comput. Coupling Phase Diagrams Thermochem. 26 (2002) 539–553.
- [37] A. van de Walle, Multicomponent multisublattice alloys, nonconfigurational entropy and other additions to the Alloy Theoretic Automated Toolkit, Calphad Comput. Coupling Phase Diagrams Thermochem. 33 (2009) 266–278.
- [38] G.L.W. Hart, R.W. Forcade, Algorithm for generating derivative structures, Phys. Rev. B. 77 (2008) 224115.
- [39] M. Yin, P. Nash, Standard enthalpies of formation of selected Rh2YZ Heusler compounds, J. Alloys Compd. 650 (2015) 925–930.
- [40] D.A. Ditmars, S. Ishihara, S.S. Chang, G. Bernstein, E.D. West, Enthalpy and Heat-Capacity Standard Reference Material: Synthetic Sapphire (Alpha-Al2O3) From 10 to 2250 K, J. Res. Natl. Bur. Stand. (1934). 87 (1982) 159.
- [41] B.H. Toby, R.B. Von Dreele, GSAS-II: the genesis of a modern open-source all purpose crystallography software package, J. Appl. Crystallogr. 46 (2013) 544–549.
- [42] G. Kim, S. V. Meschel, P. Nash, W. Chen, Experimental formation enthalpies for

intermetallic phases and other inorganic compounds, Sci. Data. 4 (2017) 170162.

[43] F. Pedregosa, G. Varoquaux, A. Gramfort, V. Michel, B. Thirion, O. Grisel, M. Blondel,
 P. Prettenhofer, R. Weiss, V. Dubourg, J. Vanderplas, A. Passos, D. Cournapeau, M.
 Brucher, M. Perrot, E. Duchesnay, Scikit-learn: Machine Learning in Python, J. Mach.
 Learn. Res. 12 (2011) 2825–2830.